Chapter 5

Tribological aspects and size effect in micromilling of Ti-6Al-4V alloy using vegetable oil based nanofluids with minimum quantity lubrication

Over the last few decades, the miniaturization of technological items has significantly impacted how people lead their lives. Size reduction enables substantially lower material expenses, increased portability, and versatility. The present micromachining technology requires a micro-scale technique capable of producing micro-components or micro-features of sizes varying from a few tens of micrometers to 1000 micrometers without any material restriction. Mechanical micro-machining becomes an alternative for the micro-scale fabrication of materials such as metals, polymers, ceramics, and composites with complex 3D features. Micromilling is the most feasible mechanical micro-machining process since it can fabricate intricate 3D micro textures, micro mold, micro components, and parts. Even though micro-milling is a popular approach for producing complicated 3D features, it has drawbacks such as significant tool wear, misalignment, and failure.

The Ti-6Al-4V alloy has been hugely employed throughout the chemical, biomedical, maritime, and aerospace industries because of its high strength, low weight, biocompatibility, and exceptional corrosion resistance. However, poor thermal conductivity, work hardening, and high chemical interaction with tool materials resulted in high surface roughness, burr formation, localized cutting temperature, and severe tool wear. Adequate lubricating techniques are required to tackle this issue. A minimum quantity lubrication (MQL) technique is a better option for efficiently distributing the lubricants/coolant while satisfying the need of being eco-sustainable to enhance cutting fluid infiltration into the narrow machining zone.

Effect of soybean oil nanofluids MQL with CuO nanoparticles and MoS_2 nanoplatelets and hybrid nanofluid (mixture of CuO and MoS_2 in the weight ratio of 90:10) MQL under micromilling conditions of Ti-6Al-4V alloy was examined concerning tool wear, surface roughness, specific cutting force, and burr formation using AlTiN coated tool has not yet been published. The measurement of percentage diameter reduction of tools, cutting edge radius enlargement, surface topography, equivalent burr width of top burr, and specific cutting forces are evaluated. The physical properties of nanofluids are examined in terms of viscosity, wettability, and nanoparticle shape morphology before performing micromilling operations.

5.1 Experimental procedure

5.1.1 Work material, coated tool, and MQL assisted micromilling

The Ti6Al4V alloy used in this experiment had sample dimensions of 55 x 50 x 5 mm, and micromilling experiments were performed on a three-axis precision micromachine center (Mikrotools DT110), and detailed specification about micromachine was given in chapter 3. Fig. 5.1 shows the experimental setup with an MQL attachment. The micro endmills considered were two flute fine grain WC with AlTiN coating thickness of 1 μm. Before performing experiments, it was ensured using scanning electron microscope (SEM) images that each microtool was defect-free and had good cutting-edge quality. Fig. 5.2 shows the AlTiN coated WC micro-mill of diameter 500 μm with its geometry properties listed in Table 5.1. Micro end-mill cutting edge radii were estimated to have a mean of 2.712 μm and a standard variation of 0.23 μm. In Table 5.2, the experimental conditions of the machining and MQL values are shown. It is clear that whenever the undeformed chip thickness value falls underneath the amount of the tool edge radius, the size effect and the influence of the minimum undeformed chip thickness may be seen. Aslantas et al. [33] revealed that the minimum chip thickness is about 0.3 times

that of the cutter corner radius for Ti6Al4V alloy. Hence, in this case, the minimum uncut chip thickness is approximately 0.81 μm/tooth. The selection of the feed per tooth resulted in the first feed being significantly below the tool edge radius where plowing is prominent and the second feed being marginally above the tool edge radius where the shearing mechanism dominates. Feed rate values are chosen for this experiment to determine the result of plowing and shearing regimes on tool wear behavior, cutting forces, surface roughness, surface topography, and burr formation. During micromilling, straight slot of 50 mm distance has been machined, 5 slots have been fabricated for each condition, and the total machining length is 250 mm. Cutting forces were measured using a piezoelectric type mini dynamometer (Kistler, 9256C2) with an accessory of charge amplifier (Kistler 5070A) and data acquisition system (Kistler, 5697) by keeping the sampling frequency at 25 kHz. Surface roughness was measured using a non-contact Zegage optical profilometer (Zygo) with a 331.63 μm × 300 μm closure area. The areal surface roughness value (S_a) was calculated by averaging the data obtained from three different locations of channels. A scanning electron microscope (SEM) captures images of the burrs, surface morphology, and tool geometry. Additionally, the picture acquired by SEM is examined using ImageJ1.52a and Axio vision software to estimate the equivalent burr width of the top burr and tool wear. As the Magnitude of the burrs shows huge variation at different locations hence instead of choosing burr width, a particular area was chosen corresponding to its height. Six different locations were taken into consideration while calculating the equivalent burr width.

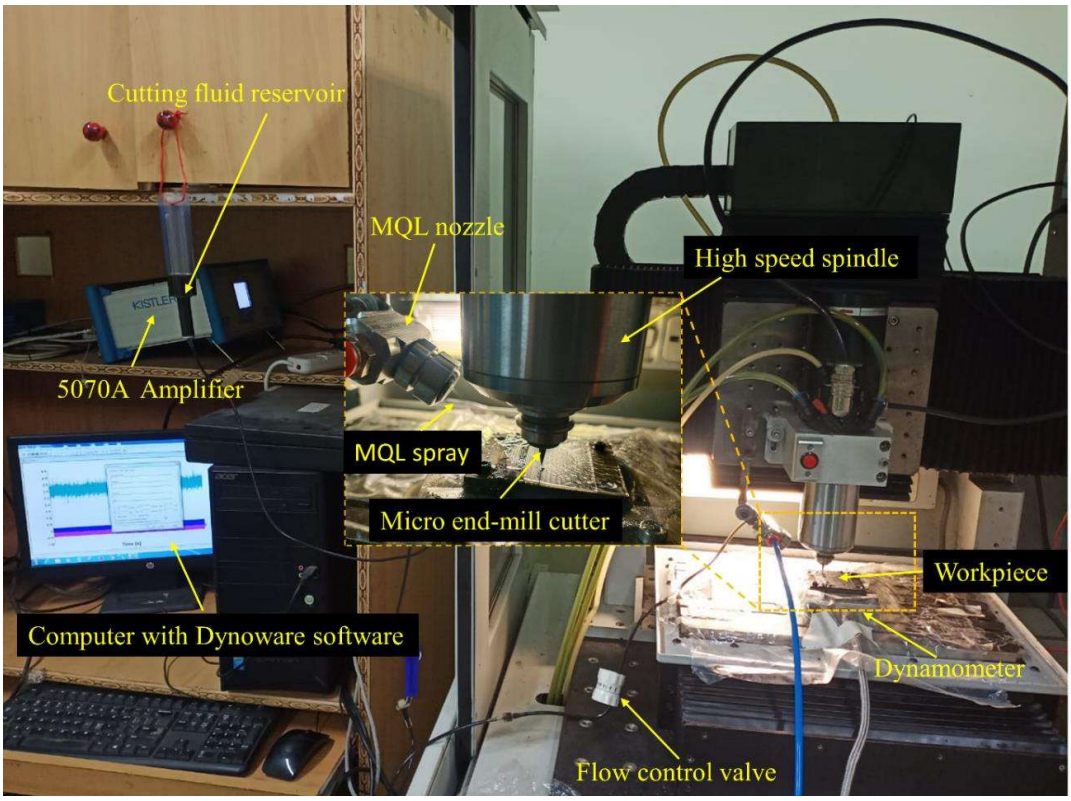

Fig. 5.1 Experimental setup using a CNC micromachining center and MQL attachment

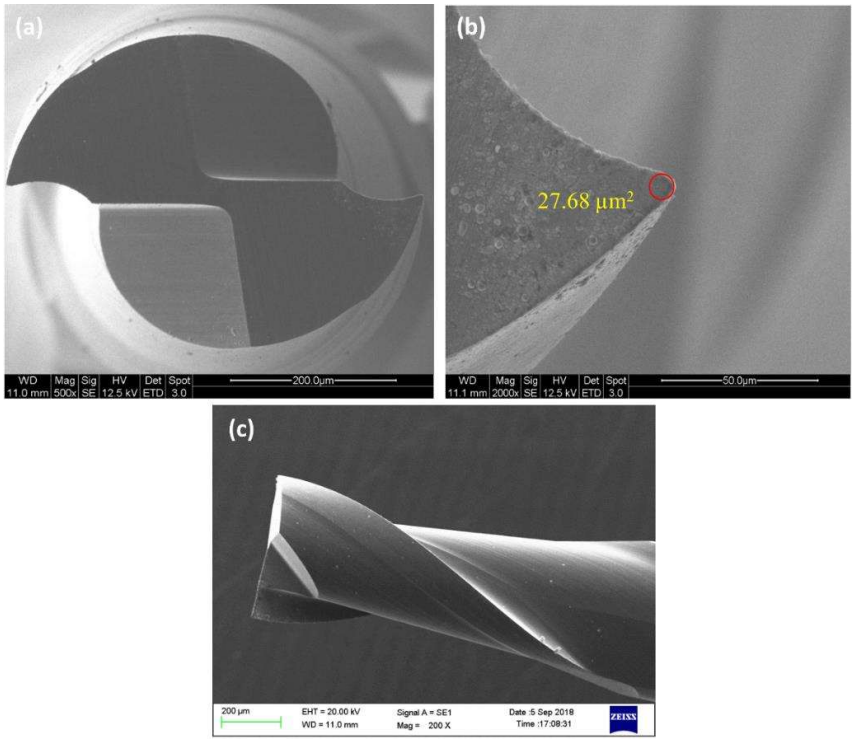

Fig. 5.2 SEM images of fresh AlTiN coated WC micro endmill (a) bottom view, (b) cutting edge radius, (c) side view

Table 5.1 Geometry of end mill cutter

Tool diameter (mm)	Edge radius (μm)	Helix angle (°)	Rake angle (°)	Clearance angle (°)
0.5	2.712 ± 0.23	30	12	9

Table 5.2 micromilling and MQL parameters

Micromilling mode	Full immersion milling
Micro endmill	AlTiN coated WC (0.5 mm diameter)
Workpiece material	Ti6Al4V
Micromilling environment	Dry, vegetable oil-based MQL, nanofluids MQL, and hybrid nanofluids MQL
Spindle speed	30000 rpm
Feed per tooth	0.3 and 4 μm/tooth
Depth of cut	60 μm
MQL flow rate	150 ml/h
MQL air pressure	4 bar
MQL nozzle distance	30 mm
The total length of cut per experiment	250 mm
Nozzle angle	45°

5.1.2 Characterization of nanoparticles and nanofluids

Nanoparticles' morphological and nanostructure features are determined using a high-resolution transmission electron microscope (HR-TEM) with low and high magnification. The sample's ethanolic mixture was dropped onto the TEM grid to capture microscopic pictures via HRTEM. As depicted in Fig. 5.3, TEM images of CuO, MoS_2, and hybrid CuO-MoS_2 nanofluids contain nanoparticles smaller than 100

nm. TEM images displayed that CuO nanoparticles are spherical without any sharp boundary, and size varies between 20-40 nm. The MoS_2 revealed a hair-like configuration appearing as a lump where the MoS_2 nanoplatelets with lateral dimensions ranging from 100-200 nm are entangled collectively. An X-ray diffraction spectrometer (Rigaku Miniflex 600 Desktop) was used to check the fabrication of CuO and MoS_2 nanoparticles. For CuO nanoparticles, all of the spikes in the XRD plot of CuO nanoparticles correspond to the JSPDS 895897 card number (Fig. 5.4 (a)). The JCPDS data card No. 75-1539 confirmed the diffraction peaks, which indicated the layered structure of MoS_2 (Fig. 5.4 (b)). The selected area (electron) diffraction (SAED) of CuO and MoS_2 nanoparticles denotes concentric rings, displaying the polycrystalline behavior of nanoparticles (Fig. 5.4 (c) and 5.4 (d)). CuO, MoS_2, and CuO-MoS_2 (weight ratio 90:10) of size less than 40 nm were dispersed in soybean oil using an ultrasonic probe sonicator. The dispersion was carried out at ambient temperature for one hour at a sonication frequency of 20 kHz and a power of 300 W. The contents of the developed nanofluids are depicted in Table 5.3. Various lubricants adopted in MQL-assisted micromilling of the workpiece are illustrated in Fig. 5.5.

Table 5.3 Composition of the prepared nanofluids

Nanofluid	Composition
MQL CuO	0.5% CuO in soybean oil
MQL MoS_2	0.5% MoS_2 in soybean oil
MQL CuO-MoS_2	0.5% CuO-MoS_2 in soybean oil
MQL Soybean oil	Soybean oil (Pure MQL)

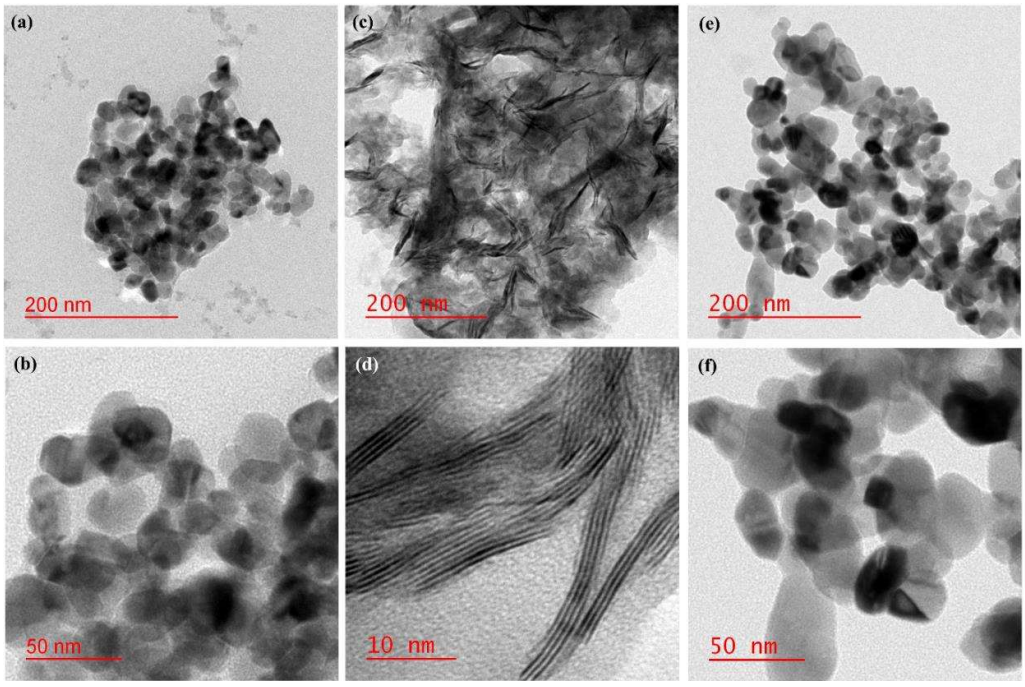

Fig. 5.3 Characterization of nanoparticles by TEM (a) & (b) CuO nanoparticles, (c) & (d) MoS_2 nanosheets, and (e) & (f) hybrid CuO-MoS_2 nanofluids

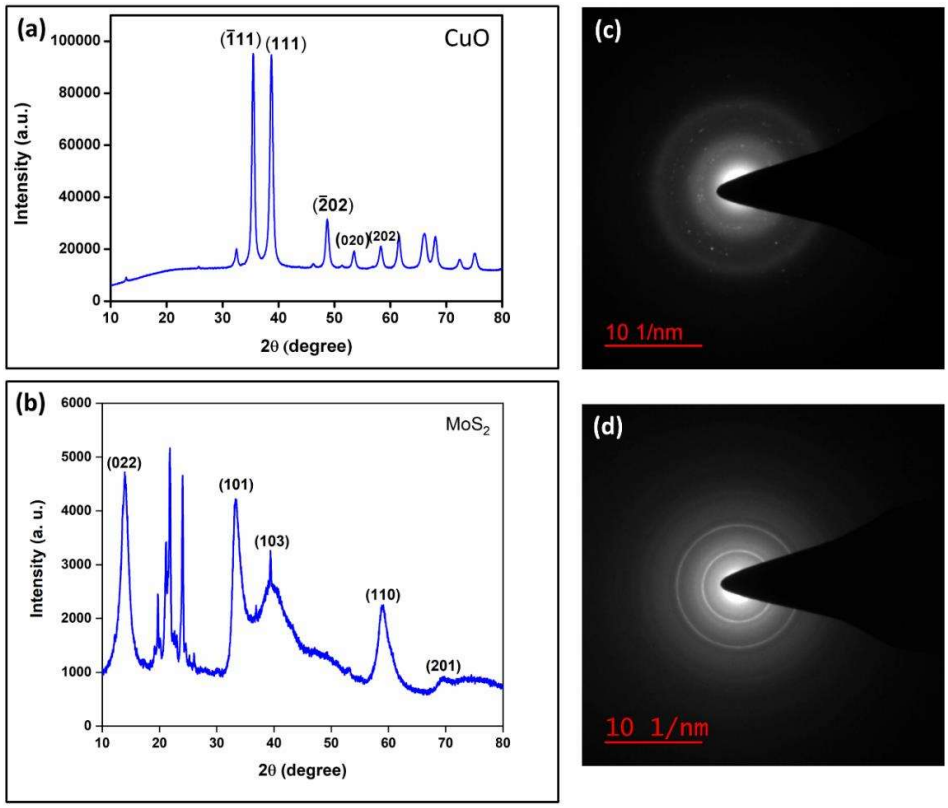

Fig. 5.4 XRD plots of (a) CuO and (b) MoS_2 nanoparticles with SAED pattern of (c) CuO and (d) MoS_2 nanoparticles showing polycrystalline rings

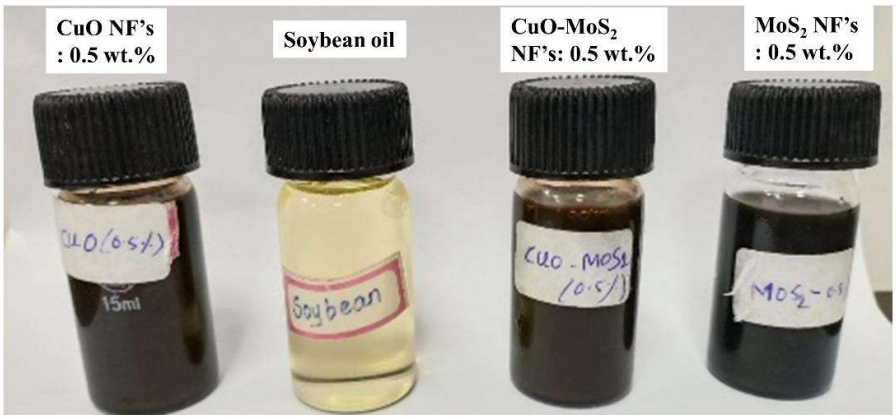

Fig. 5.5 Prepared nanofluids used in micromilling

The physical properties of cutting fluids, such as dynamic viscosity and wettability, influence how well they lubricate. The dynamic viscosity of soybean oil and nanofluids such as CuO, MoS_2, and hybrid CuO-MoS_2 (90:10) for 0.5 wt.% fraction nanoparticles was measured using a rotating viscometer (Brookfield Viscometer). Fig. 5.6 shows the dynamic viscosity of soybean oil and its nanofluids. All nanofluids show more dynamic viscosity than base liquid (soybean oil). Compared to soybean oil increment in dynamic viscosity for CuO, MoS_2 and hybrid CuO-MoS_2 nanofluids are 6.52%, 11.32%, and 13.27%, respectively.

The wettability is measured as a contact angle and is inversely proportional to the contact angle. A lower contact angle depicts better wettability to the surface. The contact angle of soybean oil and its nanofluids such as CuO, MoS_2, and hybrid CuO-MoS_2 (90:10) for 0.5 wt.% fraction nanoparticles was determined using the sessile drop technique over AlTiN coated substrate and the DSA25 contact angle measuring system Kruss (Germany). Using the sessile droplet technique, a quantity of 2 µl fluid is dropped by syringe over the substrate. The droplet size of the mist is evaluated to

determine the effectiveness of cutting fluid penetration into the confined machining zone.

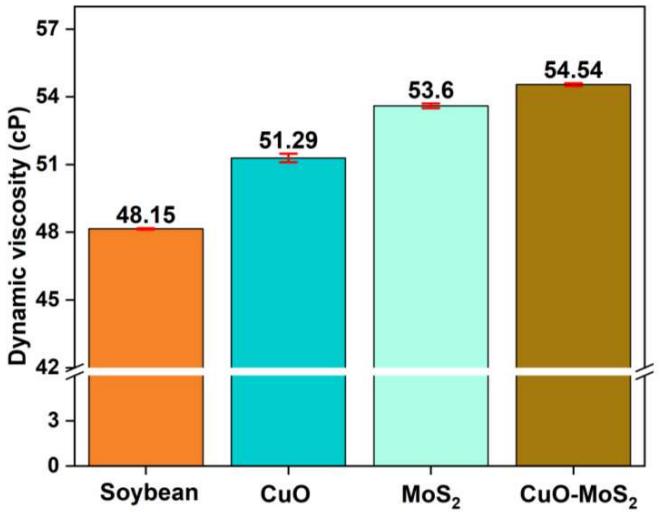

Fig. 5.6 The dynamic viscosity of soybean oil and its nanofluids

5.1.3. Micro-mist droplets measurement

In MQL, droplet size becomes critical for effective cooling and lubrication. Tiny droplets have a possibility to reach the cutting zone. This is particularly significant in micro-milling applications because of the narrow cutting surface area. Soybean oil mist is sprayed onto a clean flat glass sheet using a vertical nozzle at the following MQL mist parameters: oil flow rate of 150 ml/h, a pressure of 4 bar, and a nozzle distance of 30 mm to estimate the size of microdroplets. These parameters are also used in MQL during micromilling experiments. The diameters of 100 microdroplets were measured in the 2D image captured using a LEICA Petro-graphical microscope (Model- DM 2700 M, LEICA). Fig. 5.7 (a) shows the spherical shape of microdroplets in a microscopic image. Fig. 5.7 (c) shows the range in spray droplet size (3.16–67.51 μm). Image-J software is utilized to convert the initial image to an 8-bit mapping image to detect the droplet's shape (Fig. 5.7 (b)). Furthermore, the frequency distribution chart (refer to Fig.

5.7 (d)) reveals that most aerosols are in the 1-9 µm and 10-19 µm classes. An airborne particle size above 2 µm is preferred related to the health matters of machinists [115].

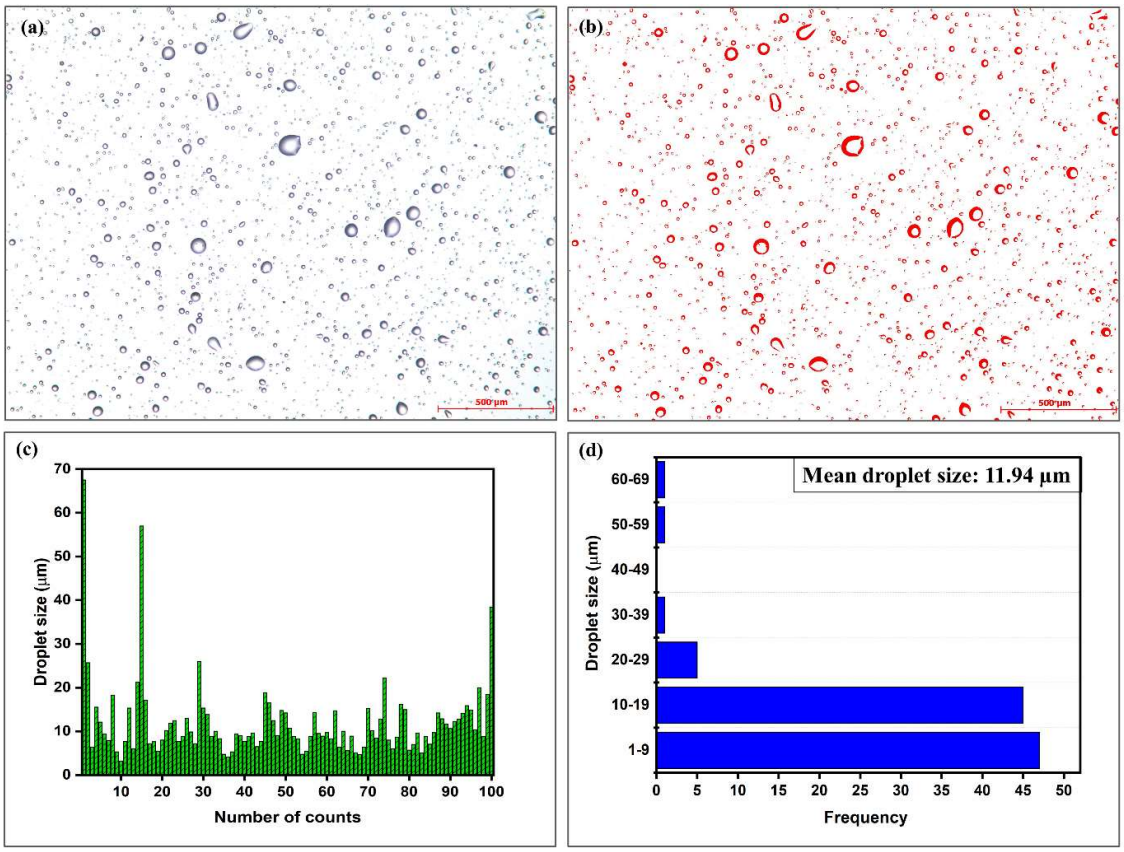

Fig. 5.7 Droplet size measurement: (a) Droplet captured image, (b) 8-Bit mapping image, (c) Droplet size variation along with the number of counts, (d) Frequency distribution of droplet size

5.1.4. Wettability test

Wettability refers to the spreadability of fluid on the workpiece and tool surface. A low contact angle improves the wettability of the liquid. Fig. 5.8 depicts the contact angle measurement between the tangent line on the droplet and the baseline on the tool surface. The wetting angle of soybean oil and corresponding nanofluids on the AlTiN coated substrate is shown in Fig. 5.9. It was noted that the contact angle of soybean oil ($37.45^{o} \pm 2.3^{o}$) is the highest of all. In contrast, the contact angle of nanofluids

decreased with the inclusion of CuO (23.48° ± 2.72°), MoS_2 (26.57° ± 1.79°), and CuO-MoS_2 (27.45° ± 1.65°) nanoparticles in soybean oil. Therefore, CuO nanofluids show the smallest contact angle and provide maximum wetting area per unit of liquid volume. Owing to the containment of nanoparticles in the thin film, the self-layering of nanoparticles encourages spreading [116].

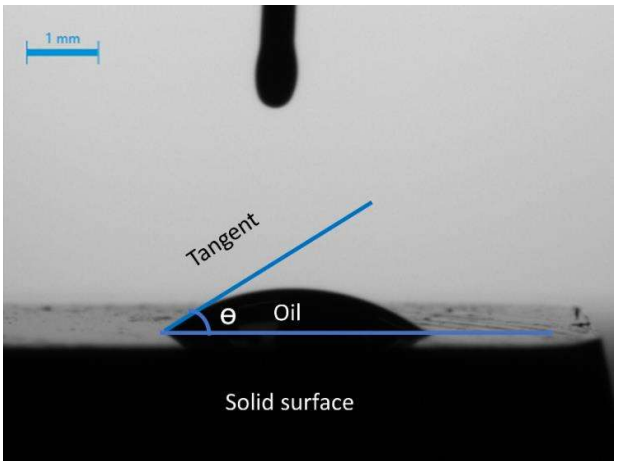

Fig. 5.8 Contact angle measurement

5.1.5. Tribology tests

Tribology tests were carried out on the nanofluids using a ball-on-disk reciprocating tribometer to assess the coefficient of friction (COF). Furthermore, the COF of lubricated surfaces of soybean oil, CuO nanofluids, MoS_2 nanofluids, and hybrid CuO-MoS_2 nanofluids compared with dry conditions was determined utilizing a WC ball with a diameter of 6 mm as a counterpart with Ti-6Al-4V plate and a 10 N normal load applied at a frequency of 3 Hz and amplitude of 2 mm during a 20 min period. For lubrication, 3 ml of soybean oil, CuO, MoS_2, and hybrid CuO-MoS_2 nanofluids were implemented on the wear track surface. Fig. 5.10 (a) illustrates the variation of the coefficient of friction with time for different lubricating conditions.

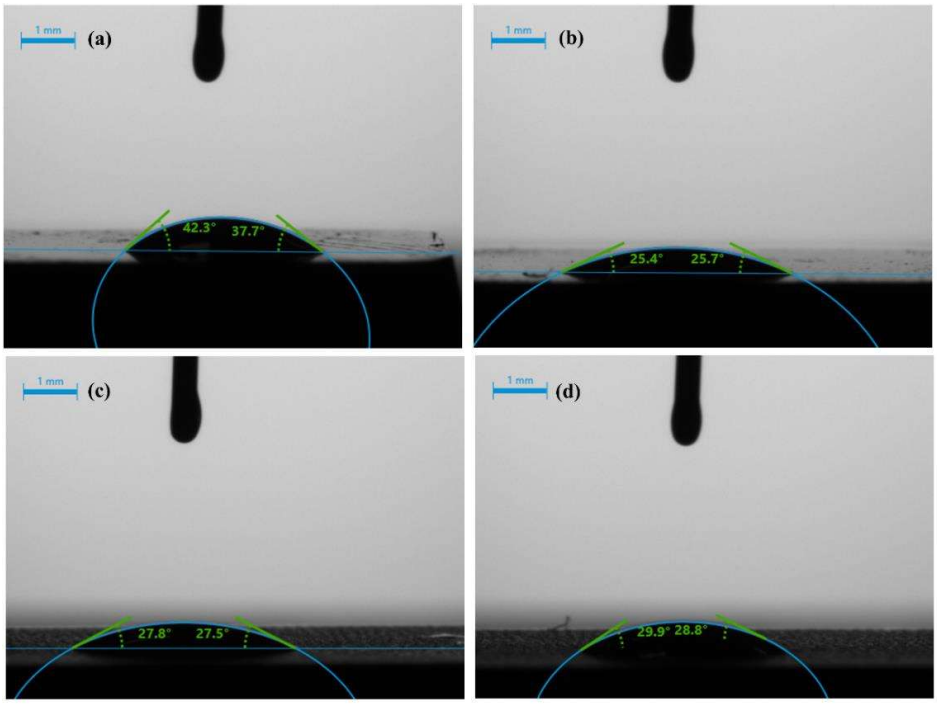

Fig. 5.9 Contact angle of (a) soybean oil and (b) CuO, (b) MoS_2 nanofluids, and (d) CuO-MoS_2 hybrid nanofluids

The most substantial decrement in COF value has been noticed for the hybrid CuO-MoS_2 nanofluid, which is less than 0.05. The dry state shows the maximum COF value, and nanofluids effectively reduce friction by rolling and self-layering (Fig. 5.10 (b)). The worn tracks' surfaces were examined using a scanning electron microscope to investigate surface morphology and deterioration in various lubricating conditions. All samples were adequately cleaned using acetone and dried before the worn surface examination to eliminate any remaining lubrication residue. SEM images of the disc's sliding surface during the ball-on-disc experiment at 500X and 2.00 KX resolution are shown in Fig. 5.11. Under dry conditions, the wear track surface shows fractured ridges and adhered wear debris, large furrows, cracks, and material adhesion due to the absence of lubrication and high heat extraction. Additionally, the adhesion wear

mechanism is the primary mechanism as symptoms of transient fusing between the rubbing surfaces at high contact temperatures caused by friction.

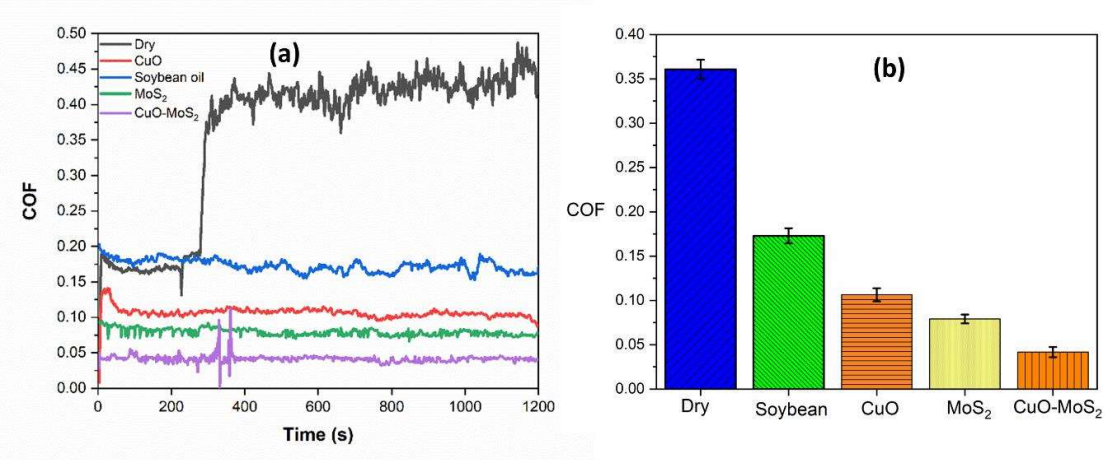

Fig. 5.10 (a) Trends of the coefficients of friction with time (b) Magnitude of coefficients of friction for different lubricating conditions

In the case of lubrication with soybean oil, the wear mechanism turns to abrasion, and micro plowing and microgrooves were observed. Therefore, the lubricating action of soybean oil has been seen as a pretty smooth surface with no severe surface defects.

Further addition of spherical CuO nanoparticles in soybean oil improves the track surface much smoother with the rolling action of nanoparticles. The contacting interface of the base fluid containing 0.5 wt% CuO is the smoothest and most compact, as shown in Fig. 5.11 (f). For MoS_2 lubrication, the rubbing region's wear trace is shinier than dry and soybean oil lubrication even though the wear furrow from 0.5 wt% MoS_2 nano lubricants was asymmetrically spread across the wear region. Hybrid CuO-MoS_2 lubricant illustrates a similar surface obtained through MoS_2 lubrication condition.

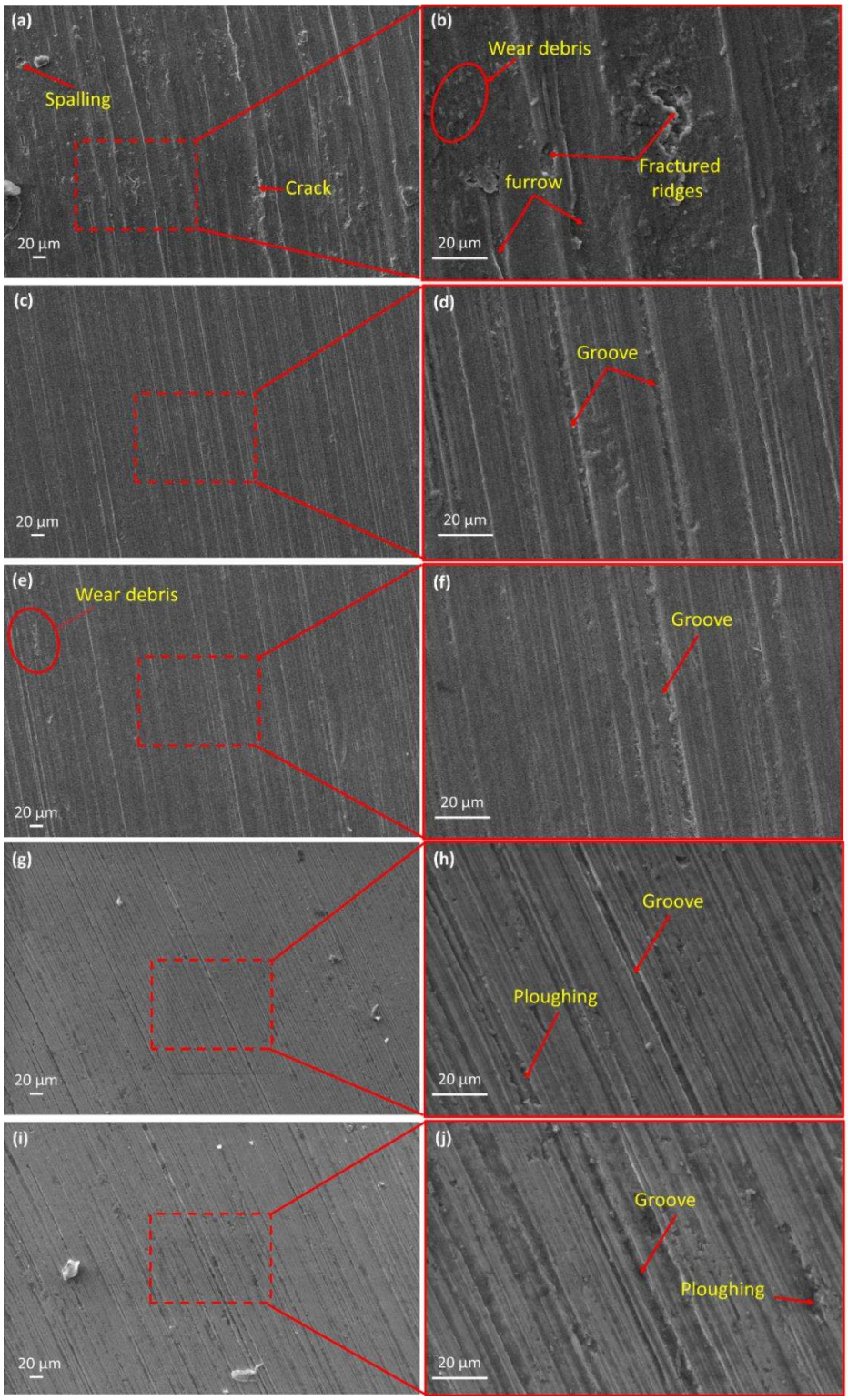

Fig. 5.11 SEM images of wear tracks under (a) & (b) dry, (c) & (d) soybean oil, (e) & (f) CuO nanofluids, (g) & (h) MoS_2 nanofluids and (i) & (j) hybrid CuO-MoS_2 nanofluids lubricating conditions

5.2 Results and discussions

5.2.1 Evaluation of tool wear and wear mechanisms

The most frequent wear phenomena in micromilling processes are flank wear, adhesion, abrasion, edge chipping, and coating delamination. Because the tool edge radius is vital in the micromilling operation, enlarging it is a crucial wear parameter to investigate in micromachining as it affects cutting forces, surface roughness, and burr formation. Micro-cutting tools are an essential aspect of mechanical micromachining; however, they are subjected to extreme circumstances, reducing tool life and negatively affecting the process costs. These conditions become more severe in the case of difficult-to-machine materials such as Ti-6Al-4V and nickel-based alloy due to poor thermal conductivity, work hardening, and reactivity towards tool materials. The assignment is to sustain the micro-mill cutting edge intact for an extended duration and prevent it from adhesion of work material and built-up edge. Hence it could be achieved using coated tool materials and minimum quantity lubrication. There are several challenges in the coating of microtools, such as the formation of droplets and enhanced cutting edge radius subjected to adhesion loss and size effect. Therefore, a thin layer of AlTiN coated material without droplet defects is utilized with different nanofluids MQL to protect the tool from abrasion, adhesion, and catastrophic failures.

Due to the tiny diameter of the tool, measuring tool wear in micro-end milling is tricky. Furthermore, no appropriate definition of tool wear for the cutting tool tip conditions in micro-end milling has yet been established. The percentage cutter diameter reduction and edge radius in plowing (0.3 μm/tooth feed) and shearing cutting (4 μm/tooth feed) regimes are carefully explored in varied cutting conditions (dry, soybean oil MQL, CuO, MoS_2, and hybrid CuO-MoS_2 nanofluids MQL). These tool wear parameters were measured using SEM images of the new and worn micro mill

after 250 mm cutting length. Further, the wear process and mechanisms are analyzed using energy-dispersive X-ray spectroscopy (EDS). Fig. 5.12 illustrates the worn microtools after machining 250 mm length under different cutting environments with 0.3 μm/tooth feed (Ploughing zone). The welded chips on the micro mill were spotted in dry condition owing to the rubbing effect of the microtool caused by the low feed per tooth and size effect, which was distinguished by no chip being produced (Fig. 5.12 (a)). Coating delamination along cutting edges and edge chipping were also observed. As shown in Fig. 5.12 (b), soybean oil MQL protects the microtool from chip debris adherence and welding by tribofilm formation. Still, it cannot prevent coating delamination and abrasion wear near the tooltip.

Further inclusion of spherical CuO nanoparticles and MoS_2 nanoplatelets lowers the coating delamination and adhesion wear. However, tools suffer fatigue due to the size effect, harsh rubbing and repetitive load, and accumulation of material unable to cut in a single milling pass. The edges of the microtools were rounded as shown for CuO nanofluids MQL condition. Fig 5.12 (e) shows a worn microtool under hybrid CuO-MoS_2 nanofluids MQL condition, and it shows oxidation wear due to poor thermo-oxidation stability of soybean oil. It has also been observed that hybrid nanofluids have the highest viscosity and poor flowability, causing the sticking of nanofluids for a longer time, and the chances of oxidation increase. Further, it was also confirmed by EDS analysis of the tool. The adhesion of work materials on the tool surface is shown by EDS analysis in Fig. 5.13 (a), and it also depicts the coating peeled off from the substrate (Fig. 5.13 (b)). The major constituents of Ti-6Al-4V alloy, Ti, Al, and V, are shown in high concentrations of 90.15%, 6.64%, and 3.22% in Fig. 5.13 (a) under dry conditions. In contrast, the primary components of tool substrates, W, C, and Co, are shown in a higher percentage in Fig. 5.13 (b) and Fig. 5.13 (c) depict spalling of

the coating in dry and CuO nanofluids MQL condition. The high percentage of oxygen is shown in Fig. 5.13 (d) for hybrid CuO-MoS_2 nanofluids MQL condition.

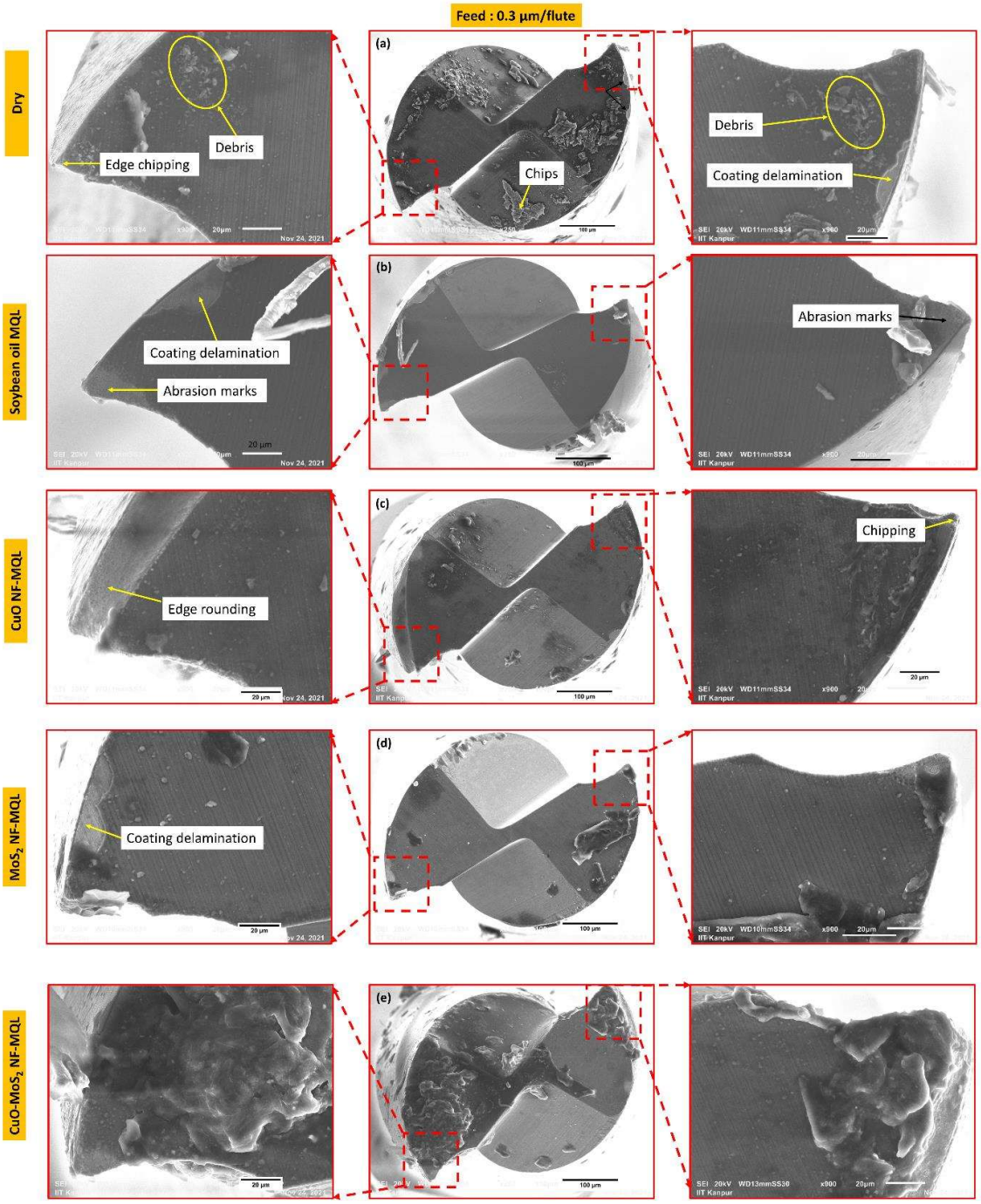

Fig. 5.12 SEM images of WC micro mill at 0.3 µm/tooth feed after cutting distance of 250 mm under (a) dry, (b) soybean oil MQL, (c) CuO NF-MQL, (d) MoS_2 NF- MQL and (d) CuO-MoS_2 NF-MQL

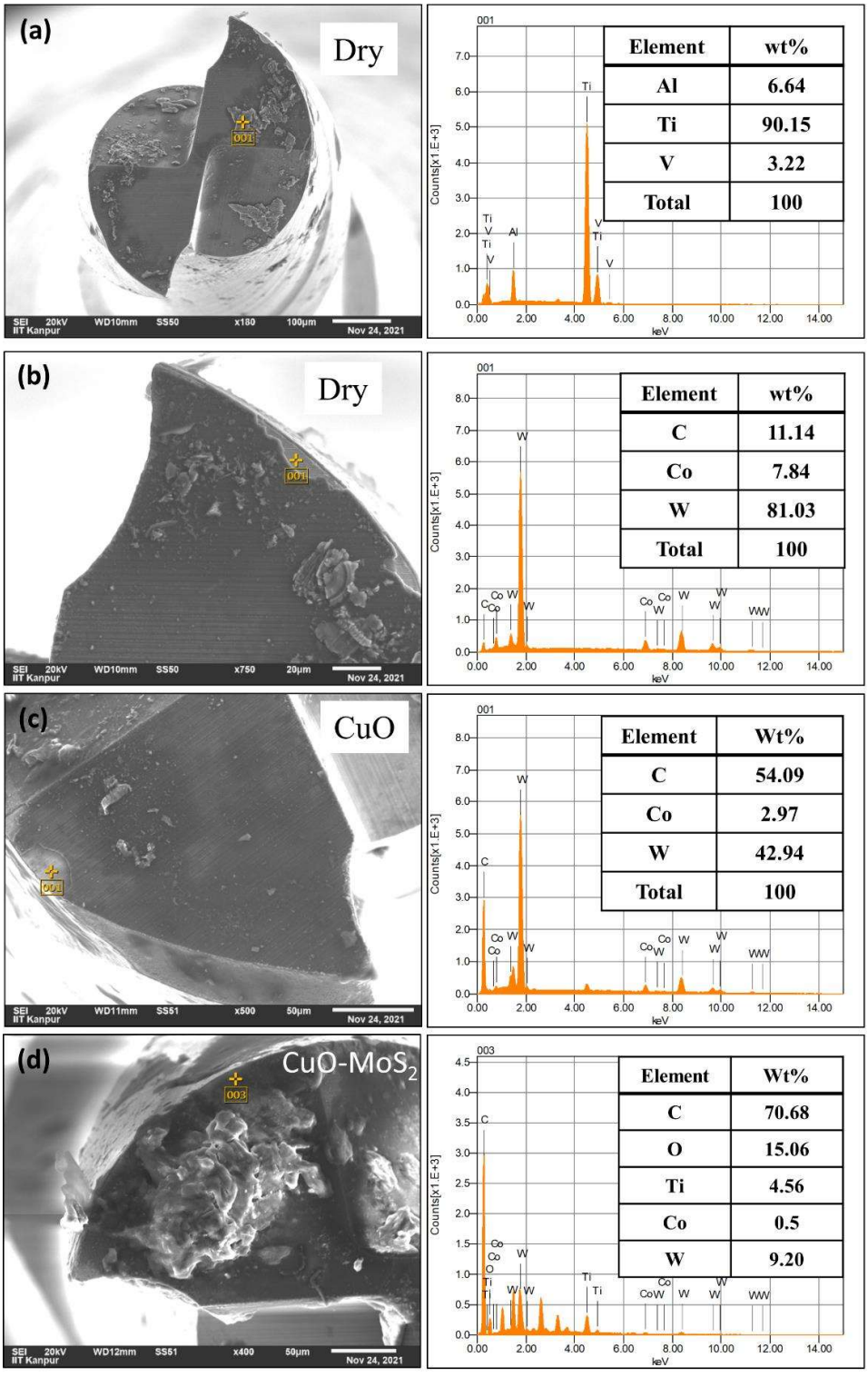

Fig. 5.13 EDS scans for AlTiN coated WC microtool at 0.3 µm/tooth feed in (a) & (b) dry, (c) CuO nanofluids MQL, and (d) hybrid CuO-MoS_2 nanofluids MQL condition

Fig. 5.14 illustrates the worn microtools after machining 250 mm length under different cutting environments with 4 µm/tooth feed (under shearing zone). The micro endmill shows the absence of severe work material adhesion at 4 µm/tooth feed compared to the plowing condition at 0.3 µm/tooth feed due to proper chip formation. However, an increase in chip load causes cutting edges to round off. Soybean oil MQL maintains the sharpness of cutting edges, although residual stress generated within the coating and repetitive cyclic load by micromilling operations cause peeling of the coating layer. Spherical CuO nanoparticles and MoS_2 nanosheets in soybean oil MQL improve the tool wear from adhesion, coating peeling off, and edge chipping (Fig. 5.14 (c) and (d)). The inclusion of small spherical CuO nanoparticles creates ball-bearing and rolling effects, forming thin tribo-films and protecting the tool from rapid wear. It also enhances thermal conductivity and heat dissipation by adding solid CuO nanoparticles with a higher thermal conductivity than base fluid [107]. CuO nanofluids also demonstrate better wettability in the contact angle measurement than other lubrication conditions. The multi-layered, weakly bonded nanostructure of MoS_2 is thought to be the cause of its superior lubricating qualities. These sheets have a low coefficient of friction and can slide against one another. Although mixing of spherical CuO nanoparticles and MoS_2 layered structures does not show synergistic effects for tool wear, as it accumulated to form larger size nanoparticles and also enhances viscosity. Further entrapment of hybrid CuO-MoS_2 nanoparticles below the tool leads to faster tool wear.

Tool wear mechanisms were analyzed using EDS after 250 mm machining length. The EDS spectra (Fig. 5.15 (a), (b), and (d)) corresponding to the locations shown under dry, soybean oil MQL, and MoS_2 nanofluids MQL conditions confirm the coating's delamination. Mainly tungsten (W), cobalt (Co), and carbon (C) are present in

the spectroscopy of Fig. 5.15 (a), (b), and (d), indicating that the AlTiN coating has been stripped from these areas. The EDS analysis of CuO and hybrid CuO-MoS_2 nanofluids MQL conditions shows a high percentage of oxygen due to poor oxidation stability of soybean oil and may also come from CuO nanoparticles.

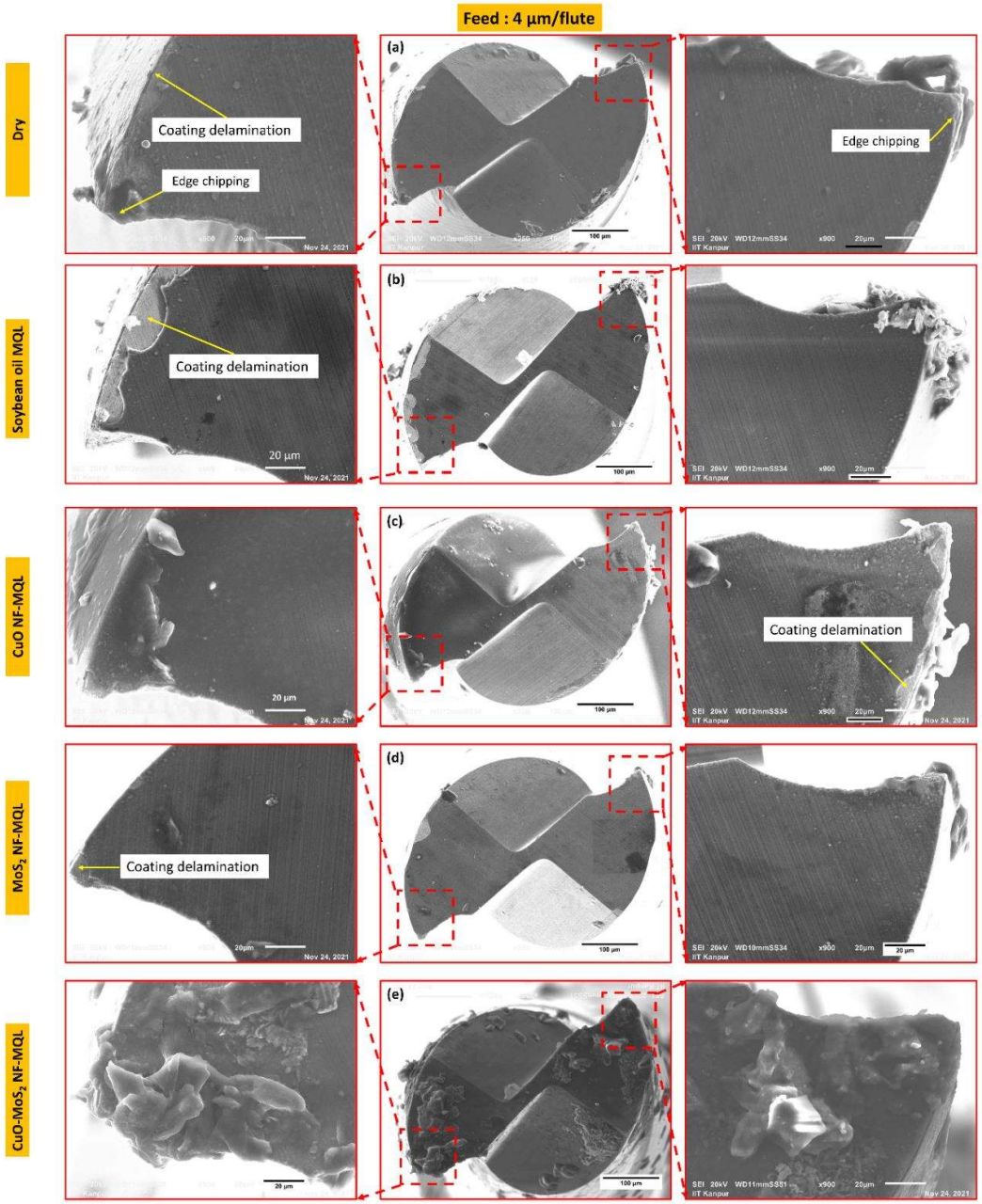

Fig. 5.14 SEM images of WC micro mill at 4 µm/tooth feed after cutting distance of 250 mm under (a) dry, (b) soybean oil MQL, (c) MQL with CuO nanofluids, (d) MQL with MoS_2 nanofluids and (d) MQL with hybrid CuO-MoS_2 nanofluids

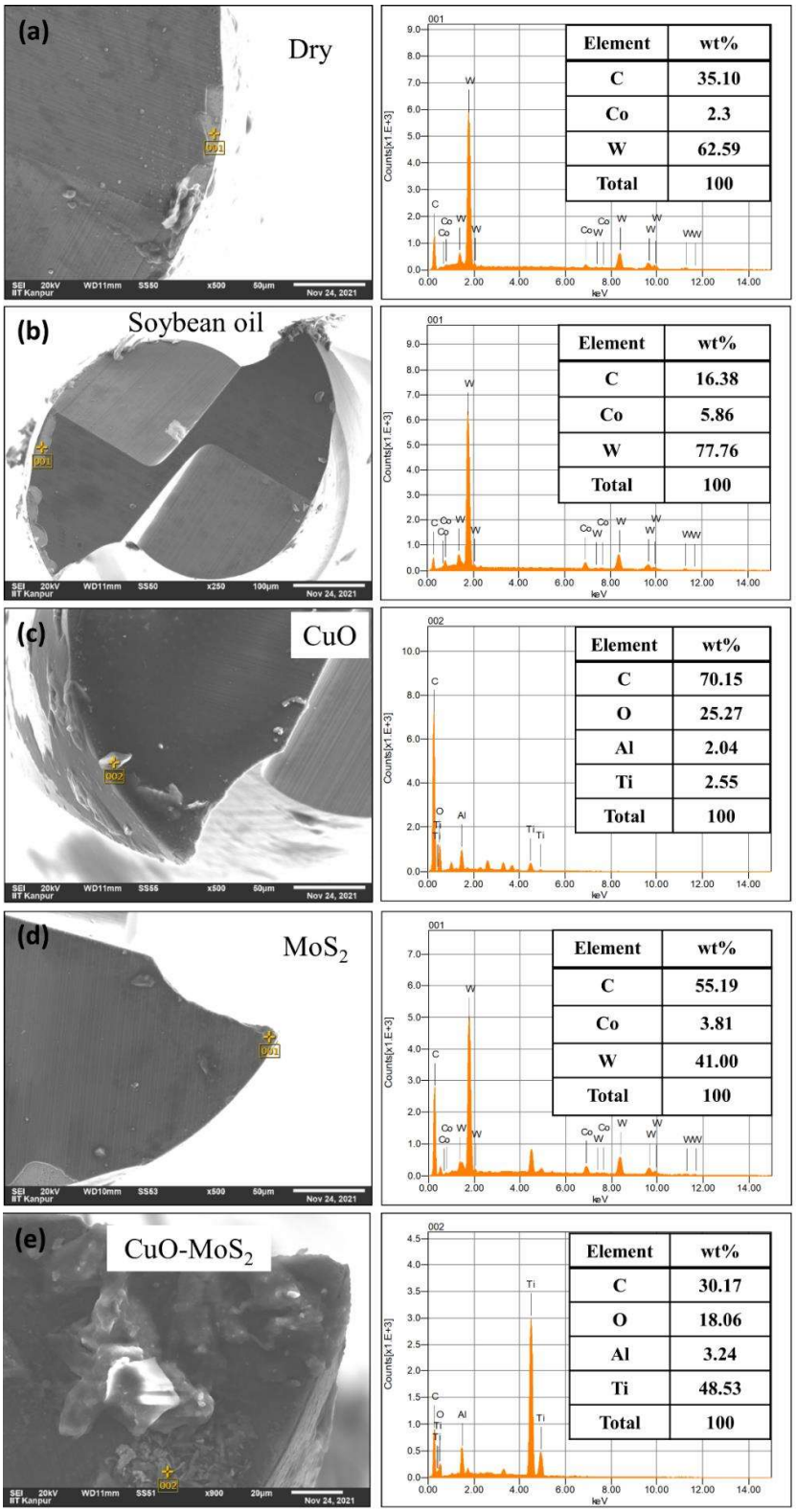

Fig. 5.15 EDS scans for AlTiN coated WC microtool at 4 μm/tooth feed rate in (a) dry, (b) soybean oil MQL, (c) CuO nanofluids MQL (d) MoS_2 nanofluids MQL and (e) hybrid CuO-MoS_2 nanofluids MQL condition

Tool wear has been assessed with respect to % diameter reduction of the tool and enlargement of cutting edge radius after evaluation of the tool wear mechanism using SEM pictures and EDS analyses. Figure 5.16 shows the % diameter reduction of micro tools and growth of cutting edge radius under various cutting conditions. Fig 5.16 (a) shows a lower % diameter reduction for MoS_2 nanofluids in the plowing zone. Other lubricating conditions do not show significant improvement regarding % diameter reduction and enhancement of cutting edge radius. In the plowing regime, small chip debris and nanoparticles are entrapped beneath the tool and propagated tool wear. Hence instead of nanofluids MQL, pure vegetable oil MQL shows a lower enlargement of edge radius.

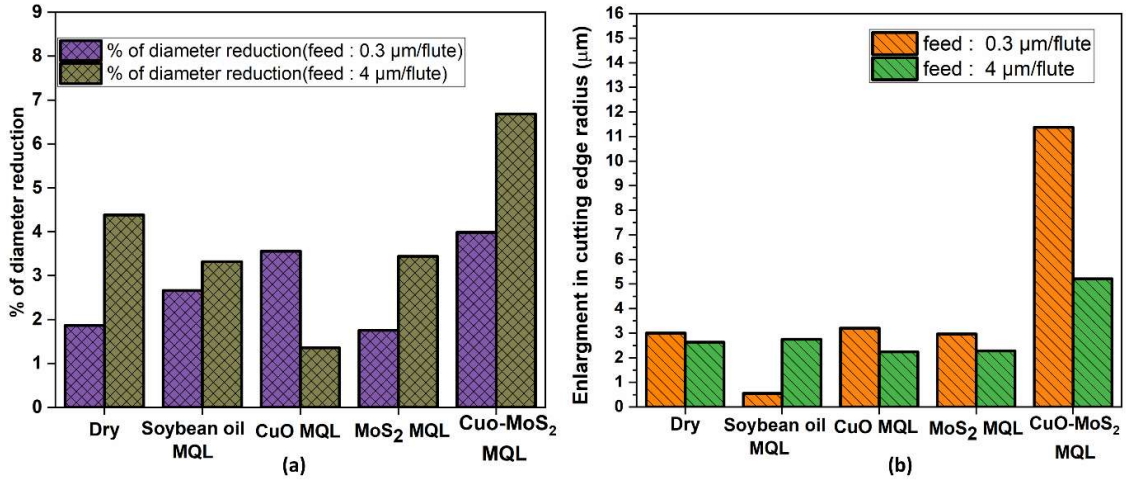

Fig. 5.16 (a) % diameter reduction of tools and (b) enlargement in edge radius

In contrast, nanofluids MQL is more significant for tool wear reduction for the shearing zone. Spherical CuO nanoparticles are more effective among nanofluids due to ball bearing, mending, and rolling effects. Oxide layer formation in hybrid CuO-MoS_2 enhances the % diameter reduction and edge radius due to the tool's chipping by removing the oxide layer near cutting edges.

5.2.2 Specific cutting force

The cutting force is connected to the dynamic features of machine tools, which include surface quality, tool wear, tool runout, and tool bending. It offers a ton of knowledge about the milling operation. Micromilling forces are commonly measured in terms of average, root mean square (RMS), and peak-to-valley (P-V) forces. Here RMS value of cutting forces is considered for comparative investigation of dry and lubricating machining. The force along the feed direction of the milling cutter is called feed force (F_X), whereas the force perpendicular to the feed direction is called cross-feed force (F_Y) (Fig. 5.17). Only cutting forces in a planar order is considered as axial force is not very significant for micromilling. Fig. 5.17 (b) and (c) denote the graph of time-dependent variation of feed and cross-feed forces during micromilling operation. Plowing force is indirectly assessed to detect a rise in specific cutting force with a decline in uncut chip thickness. The calculation of the specific cutting force requires dividing the resultant cutting force by the product of the chip load and the axial depth of cut. The resultant cutting force is determined as follows:

$$F = \sqrt{F_X{}^2 + F_Y{}^2} \tag{5.1}$$

Fig. 5.18 shows specific cutting force variation with machining length in plowing and shearing zone under different cutting environments. Much higher specific cutting force was revealed in the plowing zone compared to the shearing zone due to lower uncut chip thickness than the cutting edge radius. Both zones of dry machining show higher specific cutting force due to the absence of lubrication and a high coefficient of friction. High heat generation due to rubbing and plowing regime accelerated tool wear, generating higher cutting forces with increased machining length. The tribological characteristics of nanofluids and their impact on cutting forces are greatly influenced by their rheological properties and the structure of nanoparticles when used as a cutting fluid. In the case of plowing, highly viscous MoS_2 nanofluids for severe rubbing are

more practical owing to forming thicker lubrication film, which fills the deep grooves formed in micromilling operations. Hence least specific cutting force was obtained for MoS_2 nanofluids at 0.3 µm/tooth feed. Since there was a sharp increase in the specific cutting force of CuO nanofluids MQL after 150 mm of machining length due to edge rounding of the cutting edge or increase in cutting edge radius, variation in specific cutting force was also connected to tool wear of the micro mill. In the shearing zone, machining is not severe due to proper chip formation or the absence of plowing. Hence, spherical CuO nanofluids provide better lubrication by ball bearing and mending effect by filling up asperities on the surface. At the beginning of machining, lower viscosity cutting fluid was more influential for specific cutting force reduction; however, an increase in tool wear increased cutting force. The amount of oil atomized and deposited into the tool-chip interface depends on the viscosity of the nanofluids used in the MQL device. Hence CuO nanofluids were more beneficial for cutting force reduction in the shearing zone. The lower specific cutting force was also noted when using CuO-MoS_2 hybrid nanofluids with MQL. This is likely due to the CuO-MoS_2 hybrid nanofluid's reduced coefficient of friction, as illustrated in Fig. 5.10 (a).

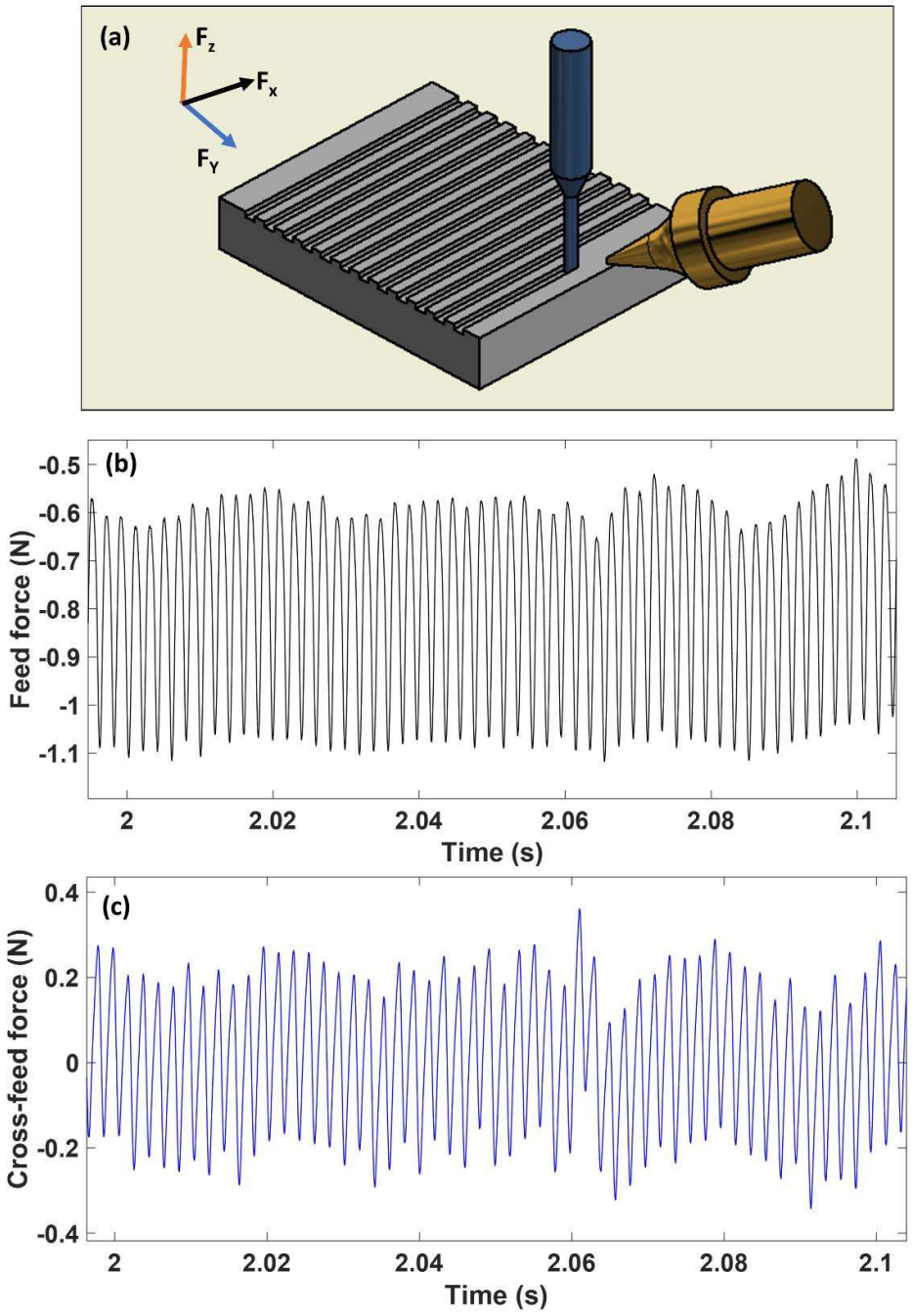

Fig. 5.17 Typical cutting forces in micromilling (a) denotes three components cutting forces (b) feed force Vs. time and (c) cross-feed force Vs. time

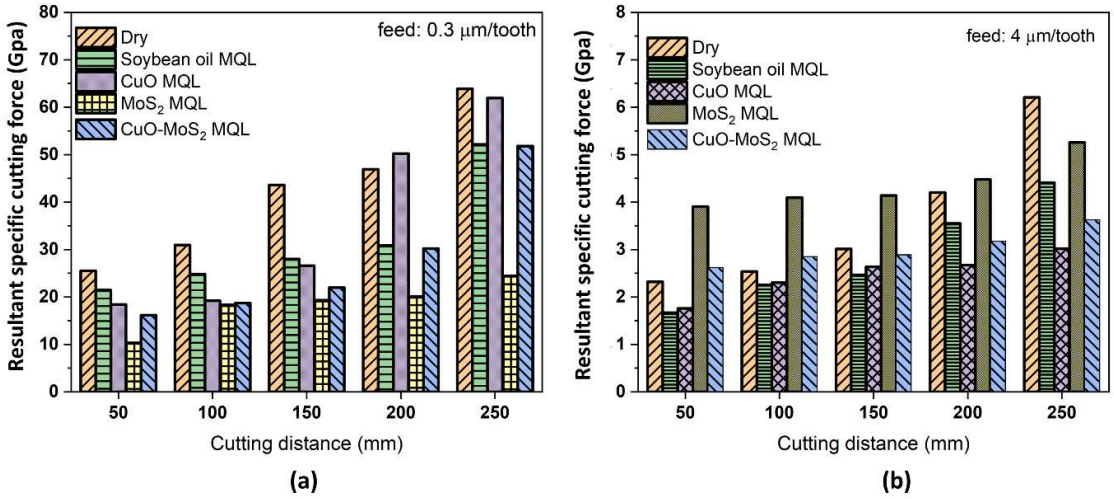

Fig. 5.18 Variation of specific cutting force at feed (a) 0.3 μm/tooth and (b) 4 μm/tooth under different environmental conditions

5.2.3 Burr formation

As deformed material, burr forms at the corners and edges of machine elements. In micromachining, burrs could be classified in a variety of methods. Burrs are categorized as entrance, exit, top, or bottom burrs based on their location. According to the causes of their generation, burrs are defined as Poisson burrs, rollover burrs, tear burrs, and cut-off burrs. The plastic side movement of the stuck material at the bottom portion of the cutting edge causes Poisson burr. It forms when deformed materials flow beneath the flank surface of microtools. A combination of Poisson and tear burr have been the most common type of top burr. Top burr is more prominent and challenging to eradicate in micromilling channels, affecting surface quality, deterioration to subsurface, accuracy, and assembly operation. Burr generation might be a problem, particularly with replicating processes like micro injection molding and hot stamping.

As observed in the SEM image of burr formation in micromilling Ti-6Al-4V alloy, there is a considerable nonuniform variation between top burr width 1 and width 2 (Fig. 5.19). As a result, estimating the width of the burr formed during the up-milling and

down-milling is extremely difficult. As a result, a new term for determining average top burr width was coined: equivalent burr width. The ratio of the total area of the burr produced to the total height of the measured slot is used. As new quantitative characteristic is obtained from the observed data, the assessment of the burrs is now more accurate. Axio vision software has been utilized to measure the area of the burr and length of the measured slot. Thus, a typical dimension of 500 µm is considered as total height. Fig. 5.19 shows that the up-milling process generates less burr than the down-milling procedure. As a result of compressing and accumulating undeformed chips during the milling operation, burrs are produced on the down-milling side. As undeformed chip thickness varies from zero to maximum in up milling and from maximum to zero in down milling, more materials accumulate and are squeezed towards the down milling side.

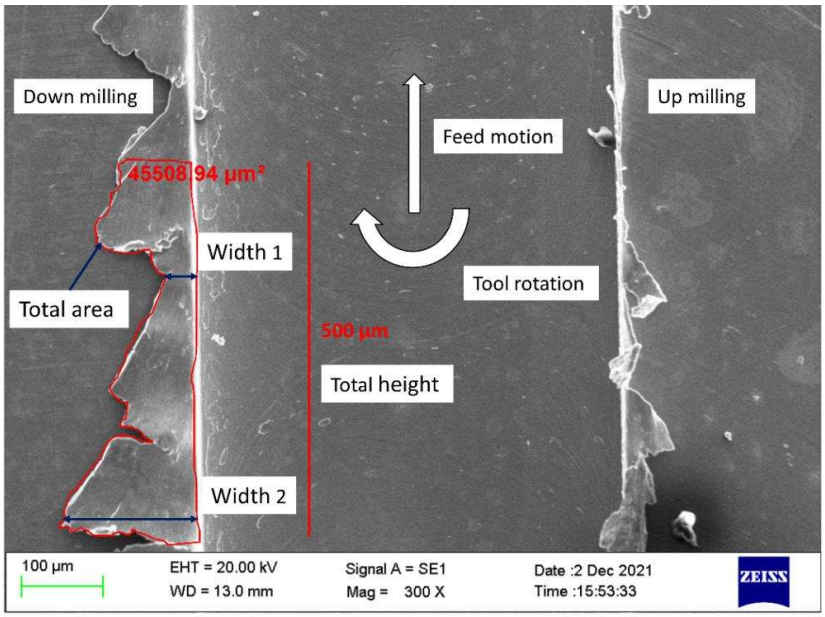

Fig. 5.19 Scanning electron microscopy (SEM) image of top burr generation in Ti-6Al-4V

Fig. 5.20 and 5.21 illustrate the top burr formation at 0.3 µm/tooth and 4 µm/tooth feed under different machining environments. Fig. 5.21 shows a large size and wavy burrs at

0.3 µm/tooth feed compared to 4 µm/tooth feed under various machining conditions due to undeformed chip thickness lower than the minimum uncut chip thickness for the given condition. Tooltip roundness or increase in edge radius is well-known to promote lower shear angle, deeper plowing, elastic deformation, and elastic recovery of micro-milled surfaces, making separation of the chips more challenging. Enlargement in edge radius for 0.3 µm/tooth feed is higher than 4 µm/tooth feed, producing thicker and wavy burrs. As observed in Fig. 5.20 (a) and Fig. 5.21, 0.3 µm/tooth feed depicts the lowest burr width for soybean oil MQL condition due to lower edge radius enhancement shown in Fig. 5.16 (b). Due to the size effect, the plowing action at 0.3 µm/tooth feed will take more considerable material to reach the machined surface via the flank face underneath the stagnation point. These materials could not form chips, resulting in a Poisson burr or top burr. At 4 µm/tooth feed uncut chip thickness above the cutting edge radius, proper chip formation takes place, and for the most portion, material moves upward, generating chips. The growth of burrs is caused by little material protrusions to the side. As observed in Fig. 5.20 (b) and Fig. 5.21, 4 µm/tooth feed depicts the lowest burr width for CuO nanofluids MQL condition due to lower edge radius enhancement shown in Fig. 5.16 (b).

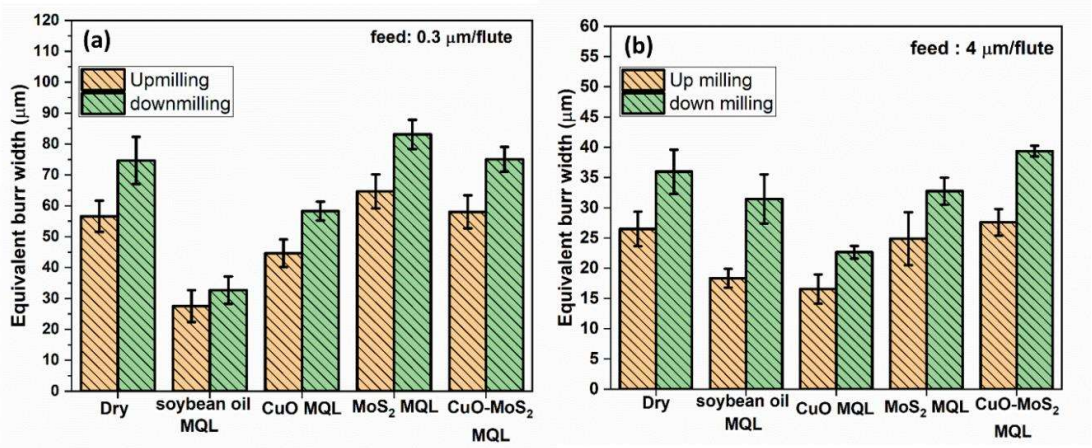

Fig. 5.20 Magnitude of equivalent top burr width in (a) plowing zone and (b) shearing zone under different lubrication conditions

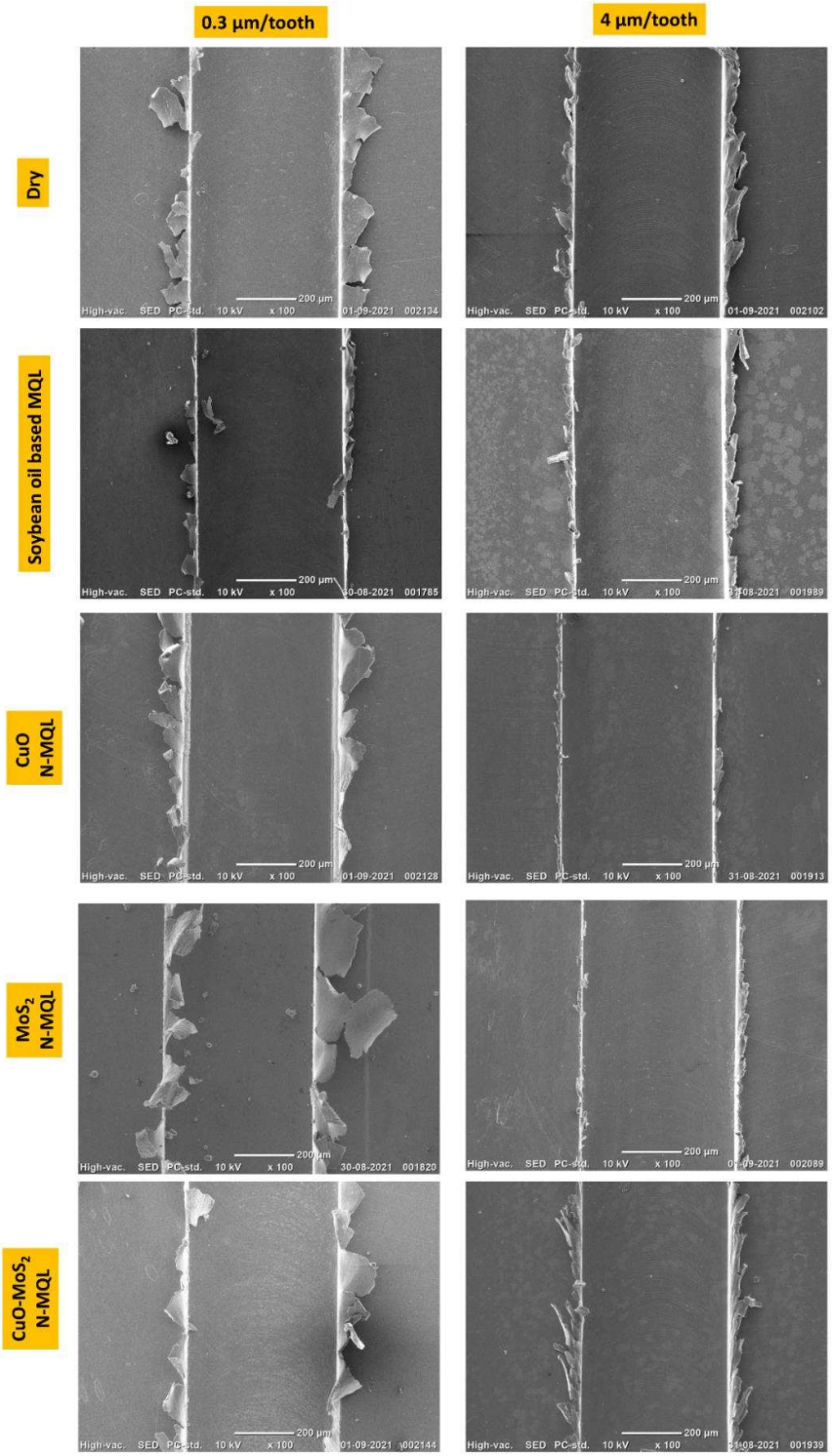

Fig. 5.21 Burr formation in plowing and shearing conditions with the cutting length in between 200 and 250 mm under different cutting environments

5.2.4 Surface roughness and surface topography

In different cutting environments, Fig. 5.22 displays the 2D and 3D surface topography of the micro-slot mid-region at 0.3 μm/tooth feed. From Fig. 5.22, it can be seen that in dry conditions larger amount of material debris accumulated on the machined surface. These accumulations of material debris were also found on the micro end-mill utilized in a dry condition, as shown in Fig. 5.12. Thus, at 0.3 μm/tooth feed, ploughing was the predominant cutting mode used to machine the workpiece's material, producing a rougher surface and the deposition of material debris that could not become chips. Due to the high heat generation in a dry environment, tool chipping, and accelerated tool wear development, several nonuniform feed marks with minor heaves could be seen on the surface. This uneven surface and material debris deposition produce higher surface roughness than other cutting conditions. Through spray flushing and heat dissipation, the MQL technique with vegetable oil dramatically lowers the amount of material debris that accumulates on machined surfaces. However, uneven feed marks were also found in soybean oil MQL due to ploughing action, and lower surface roughness was achieved than in dry conditions. Spherical CuO nanoparticles improve surface topography due to the absence of chip debris on the bottom surface of the microchannel by different mechanisms like ball-bearing, rolling, and mending. The inclusion of nanoparticles improves wettability and viscosity, which provides more considerable heat dissipation and stable tribofilm. Mono nanofluid MQL consisting of single nanoparticles during micromilling considerably enhanced surface morphology compared to dry and vegetable oil MQL-assisted machining, primarily because of the spherical shape of the CuO nanoparticles. Among all cutting conditions, hybrid CuO-

MoS_2 nanofluid produces the best surface topography with lower surface roughness. It is anticipated that friction is significantly reduced by the synergistic effect produced by the spherical CuO and the lamellar MoS_2, as well as the improvement in the effectiveness of the interfacial slipping action mechanism. As an outcome, when compared to a dry machining condition, the areal surface roughness (S_a) was lessened by about 38.6%, 50.8%, 40.7%, and 52.9% using soybean oil MQL, CuO, MoS_2, and hybrid CuO-MoS_2 nanofluids MQL.

In different milling conditions, Fig. 5.23 displays the 2D and 3D surface topography of the micro-slot middle portion at 4 μm/tooth feed. In the existence of plastic side flow and shallow grooves, dry micro-milling has resulted in the most surface defects because of the lack of lubrication and direct tool-to-workpiece contact, which promotes damage. However, the application of soybean oil MQL reduces the intense plastic deformation and side flow and shows evenly distributed feed marks. In comparison to other cutting conditions, the surface topographies in Fig. 5.23 show that micromilling with the CuO nanofluid and hybrid CuO-MoS_2 nanofluid MQL considerably decreased the milling marks and the areal surface roughness. This is described by the ball-bearing ability of CuO nanoparticles, which fills in pores to minimize interaction, and MoS_2's considerable load-carrying capability generates minimal sliding resistance to reduce friction on surface contact [117, 118]. As an outcome, when compared to a dry machining condition, the areal surface roughness (S_a) was lessened by about 32.12%, 47.3%, 38.8%, and 55.1% using soybean oil MQL, CuO, MoS_2, and hybrid CuO-MoS_2 nanofluids MQL. With hybrid CuO-MoS_2 nanofluid as the lubricating condition, the superior surface topography was thus obtained at 0.3 μm/tooth and 4 μm/tooth feed.

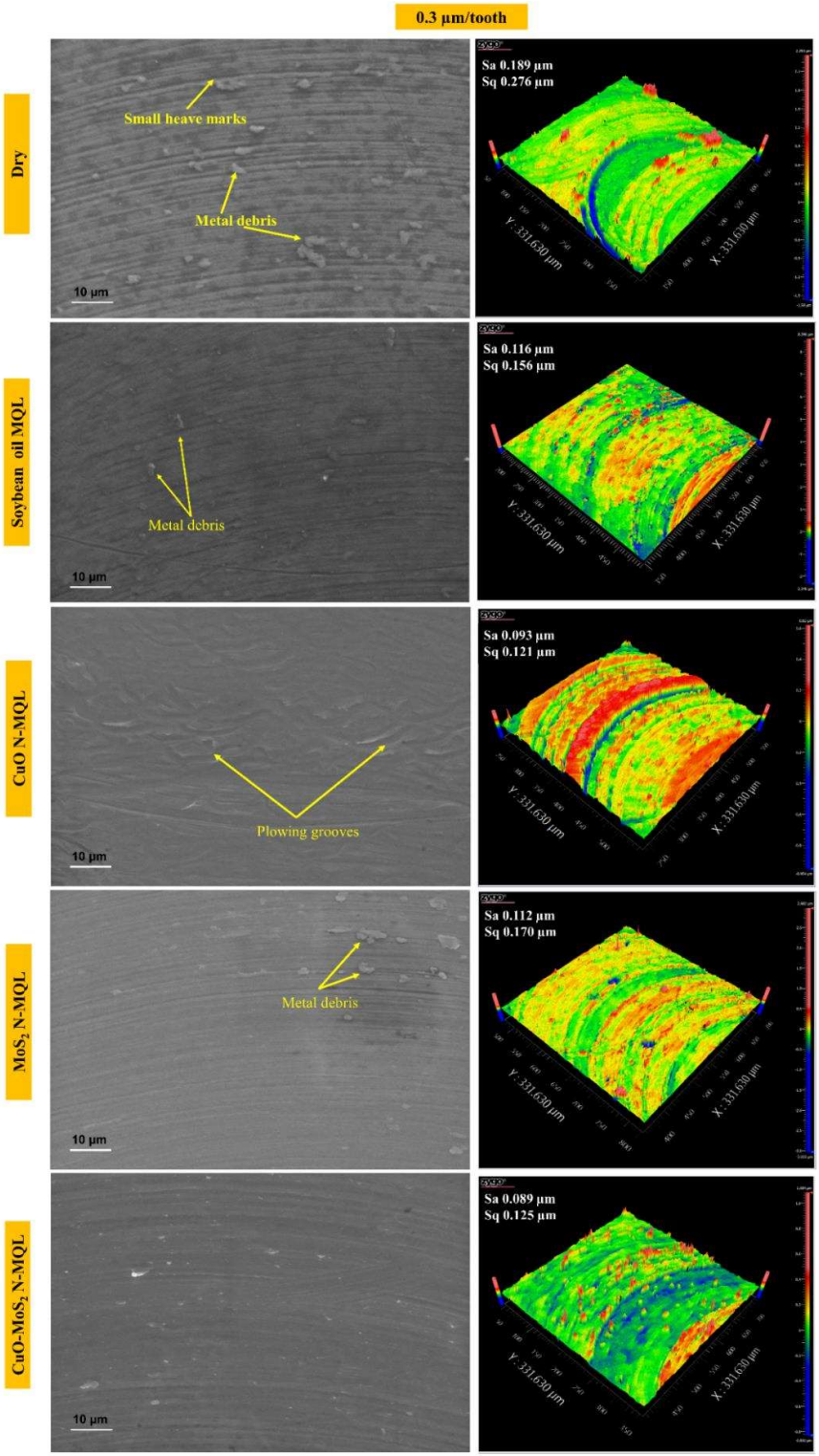

Fig. 5.22 Surface topography and surface roughness of the micro-slot mid-region at 0.3 µm/tooth with the cutting length between 200 and 250 mm under different machining environments

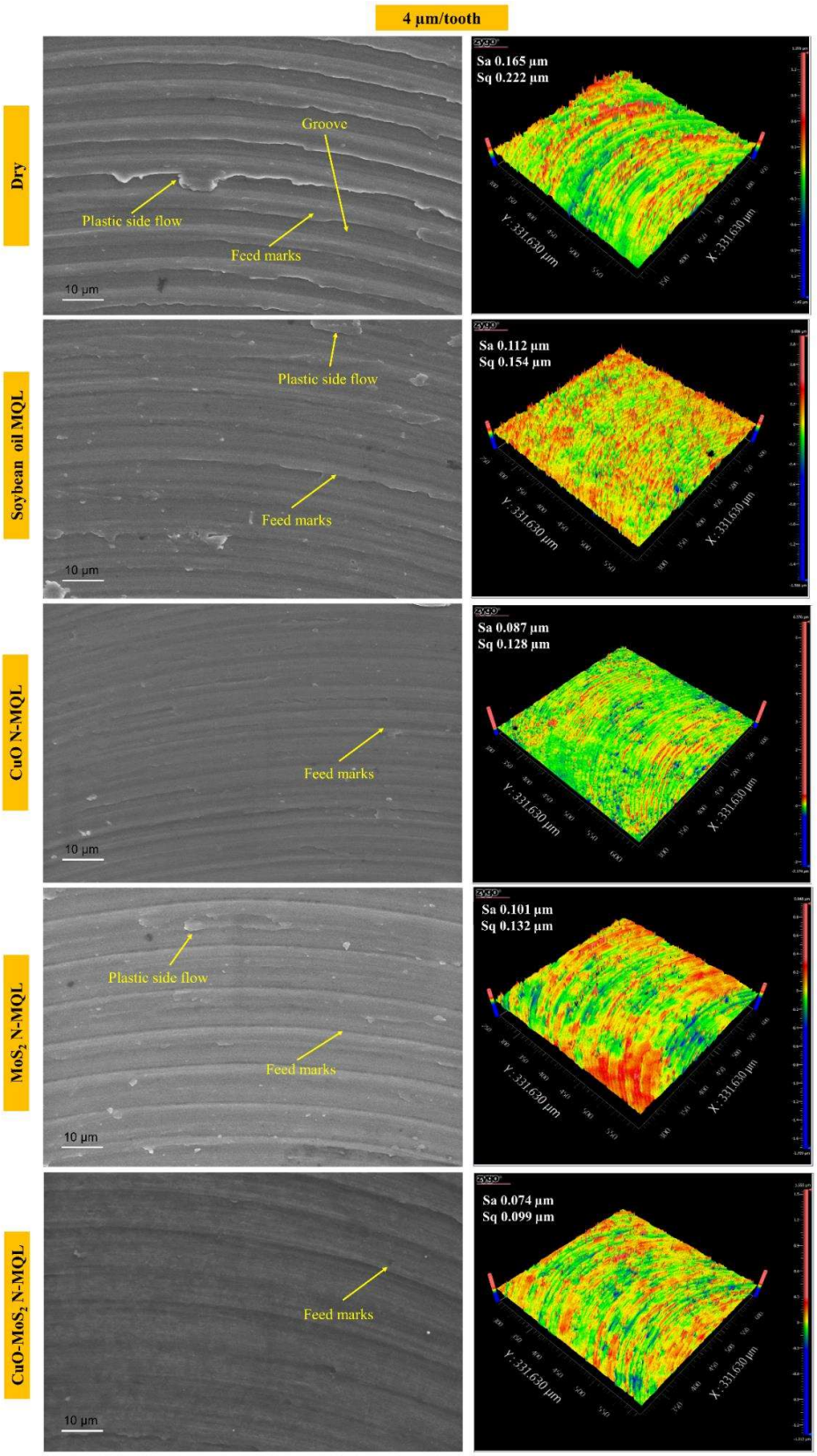
4 µm/tooth
Dry
Groove
Plastic side flow
Feed marks
10 µm
Sa 0.165 µm
Sq 0.222 µm
Soybean oil MQL
Plastic side flow
Feed marks
10 µm
Sa 0.112 µm
Sq 0.154 µm
CuO N-MQL
Feed marks
10 µm
Sa 0.087 µm
Sq 0.128 µm
MoS2 N-MQL
Plastic side flow
Feed marks
10 µm
Sa 0.101 µm
Sq 0.132 µm
CuO-MoS2 N-MQL
Feed marks
10 µm
Sa 0.074 µm
Sq 0.099 µm

Fig. 5.23 Surface topography and surface roughness of the micro-slot middle region at 4 µm/tooth feed with the cutting length between 200 and 250 mm under different machining environments

5.3 Summary

This chapter aims to identify the appropriate lubricant that can be used for efficient micromilling of Ti6Al4V alloy and to evaluate micromilling performance in terms of tool wear, specific cutting force, burr formation, surface roughness, and surface topography. From the study, the key finding can be summed up as follows:

- It has been observed that wettability and dynamic viscosity are enhanced by adding CuO nanoparticles and MoS_2 nanoplatelets. Vegetable oil's dynamic viscosity is increased by 6.12%, 10.17%, and 11.72%, respectively, by the addition of CuO, MoS2, and CuO-MoS2 nanofluids. The contact angle of nanofluids on AlTiN coated WC substrate decreased with the inclusion of CuO (23.48^o), MoS_2 (26.57^o), and CuO-MoS_2 (27.45^o) nanoparticles in soybean oil (37.45^o).
- The minimum coefficient of friction of magnitude below 0.05 and smooth wear tracks was obtained using hybrid CuO-MoS_2 nanofluids at 0.5 wt.% concentration.
- Areal surface roughness measured was lowest for hybrid CuO-MoS_2 nanofluids than other lubricating conditions at 0.3 µm/tooth and 4 µm/tooth due to the combined effect of rolling and shearing by CuO nanoparticles and MoS_2 nanoplatelets. Surface topography has also shown smoother with fewer feed marks and surface defects for hybrid nanofluids.
- The areal surface roughness (S_a) at 0.3 µm/tooth was lessened by about 38.6%, 50.8%, 40.7%, and 52.9% using soybean oil MQL, CuO, MoS_2, and hybrid CuO-MoS_2 nanofluids MQL compared to dry conditions. Similarly, at 4

μm/tooth, areal surface roughness (S_a) reduce by about 32.12%, 47.3%, 38.8%, and 55.1% using soybean oil MQL, CuO, MoS_2, and hybrid CuO-MoS_2 nanofluids MQL than dry conditions.

- In dry micromilling with 0.3 μm/tooth feed, adhesion of the chip was observed both on the bottom of the WC microtool surface and cutting edges.
- For the ploughing regime at 0.3 μm/tooth feed, soybean oil MQL reduces tool adhesion through proper lubrication.
- For the shearing regime at 4 μm/tooth feed, CuO NF-MQL and MoS_2 NF-MQL were found more effective for adhesion wear than vegetable oil MQL and dry conditions.
- For the shearing regime at 4 μm/tooth feed, CuO NF-MQL and MoS_2 NF-MQL were found more effective for adhesion wear than vegetable oil MQL and dry conditions. However, for the plowing regime at 0.3 μm/tooth feed, pure soybean oil MQL reduces tool adhesion through proper lubrication.
- Enlargement in edge radius for 0.3 μm/tooth feed is obtained higher than 4 μm/tooth feed for dry, CuO, MoS_2, and CuO- MoS_2 nanofluids MQL except for soybean oil, and percentage enlargement for cutting edge radius was 12.37%, 29.99% 23.18 and 54.23% respectively. Enlargement in edge radius owing to 0.3 μm/tooth than 4 μm/tooth feed resulting larger size wavy and thicker burrs in down milling that cause percentage enlargement of equivalent burr width for dry, soybean oil, CuO, MoS_2, and CuO-MoS_2 nanofluids MQL by 51.85%, 3.76%, 61.12%, 60.61%, and 47.54% respectively.
- At a feed of 0.3 μm/tooth, MoS_2 nanofluids produced a lower specific cutting force. In contrast, at a 4 μm/tooth feed, CuO nanofluids significantly reduced specific cutting force.